Mapping the Human Blood-Retinal Barrier Function

Rui Bernardes*, Jorge Dias, and José Cunha-Vaz

***Abstract*—The aim of the work herein presented is to map blood-retinal barrier function by measuring retinal fluorescein leakage from the blood stream into the human vitreous using a confocal scanning laser ophthalmoscope (CSLO). Existing methods for the assessment of fluorescein leakage into the human vitreous are based on the qualitative evaluation of fluorescein angiographies (FA) and on volume measurements, as performed by the Fluorotron Master. A new procedure is presented capable of measuring fluorescein leakage into the vitreous while simultaneously imaging the retina. The present methodology computes the fluorescein leakage in a fully automated way, based on the three-dimensional fluorescence distribution in the human eye by using a single data acquisition. The processing includes signal filtering, volume alignment and profile deconvolution. The deconvolved profile obeys the established physical model. Representative cases shown are: a healthy eye; an eye with drusen from a nondiabetic person; a photocoagulated eye; and an eye with nonproliferative diabetic retinopathy. The results are in agreement with previous findings and go a step further by making possible its daily usage in a clinical setup based on currently available instrumentation.**

***Index Terms*—Blood-retinal barrier, diagnosis, fluorescein leakage, functional imaging, ophthalmology, retinal mapping.**

I. Introduction

THE AIM of the work presented in this paper is to compute the leakage of fluorescein occurring from the blood retinal circulation into the human vitreous, *in vivo*. This leakage is directly related to the blood-retinal barrier (BRB) permeability to fluorescein. Because this barrier is affected by diabetes and a variety of other retinal diseases associated with progression to blindness, it is particularly important that its function is assessed and monitored.

Diabetic retinopathy (DR), i.e., alterations on the retina due to diabetes, is the leading cause of legal blindness in developed countries. In the USA, there are 100 000 new cases each year, while in the European Union it is expected that by the year 2010, 10% of the population will develop diabetes [1]. This disease mainly affects the active working population aged 24 to 74 years old [2], the reason why it has such a large socio-economic impact. The changing world demography of type 2 diabetes involving increased numbers of patients in developing countries will make diabetic retinopathy a real global health issue [3].

Several multicentric studies were established to deal with this problem. Among them are the Diabetic Retinopathy Study (DRS), Early Treatment Diabetic Study Group (ETDRS), the Diabetes Control and Complications Trial (DCCT), and the United Kingdom Prospective Diabetes Study (UKPDS).

Manuscript received October 22, 2003; revised May 25, 2004. *Asterisk indicates corresponding author.*

*R. Bernardes is from the Centro de Novas Tecnologias para a Medicina da Associação para a Investigação Biomédica e Inovação em Luz e Imagem (AIBILI/CNTM), 3000-548 Coimbra, Portugal (e-mail: rcb@aibili.pt).

J. Dias is with the Departamento de Engenharia Electrotécnica e de Computadores da Faculdade de Ciências e Tecnologia da Universidade de Coimbra, 3000-290 Coimbra, Portugal.

J. Cunha-Vaz is with the Faculdade de Medicina da Universidade de Coimbra, 3000-548 Coimbra, Portugal.

Digital Object Identifier 10.1109/TBME.2004.839801

Fig. 1. Digital FA of a diabetic patient taken 30.7 s after intravenous fluorescein administration.

Clinical criteria for the evaluation of the DR were established by the ETDRS group and these criteria, mostly based on fundus photography, remain in use in the ETDRS protocol. Fluorescein angiography (FA) consists on the photographic registration of the passage of fluorescein in the retinal circulation after its intravenous administration and identifies better the morphology of the open retinal vasculature and sites of fluorescein leakage.

In this paper, we present a *quantitative* method for BRB assessment, useful for clinical evaluation of the DR and follow-up studies. A prototype software system for generation of BRB functional maps has been implemented and tested under a variety of clinical situations and retinal morphologies.

Although applied to different instrumentations, the method herewith presented pursues the same objectives of the work presented in [4], but describes the procedure that allows detailed mapping of the BRB using currently available instrumentation.

To our knowledge, the current work and the work presented in [5] are the only approaches for computing fluorescein leakage from the blood stream into the human vitreous, *in vivo*, by means of three-dimensional (3-D) volumetric information with simultaneous imaging of the retina, thus establishing a direct correlation between retinal leakage and retinal morphology.

II. Material and Methods

The photographic registration of the passage of sodium fluorescein in the retinal circulation is called FA. An example of a digital FA, taken 30.7 s after dye administration, can be seen in Fig. 1.

Sodium fluorescein is a dye (Sodium Fluorescein, NaFl, $C_{20}H_{10}O_5Na_2$) that is used clinically because of its nontoxic properties, fluorescence levels and dimension of molecules (376 Daltons).

The rationale behind fluorometry is the fact that sodium fluorescein, simply referred to as fluorescein from here on, enters healthy eyes in minimal quantities, penetrating at much faster rates in diseased eyes. Its spectrum has a peak of absorption at 490 nm and a peak of emission at 515 nm [6].

In 1975, an important step was taken for the assessment of the BRB: the application of fluorophotometry to the clinical study of posterior segment disease [7], [8]. Others followed [9], [10].

For a brief history on ocular fluorophotometry see [11].

Instrumentation was developed to compute a number that indicates an average value for the permeability index of the BRB to fluorescein. The instrument, named Fluorotron Master, is made by OcuMetrics Inc. (Mountain View, CA) and details can be seen in [12]–[14]. Nevertheless, this system can only provide a single measure for the entire posterior pole of the eye. Still, it made possible an objective comparison between different patients and/or monitoring of the same patient over time. A Confocal Scanning Laser Ophthalmoscope (CSLO) instrument is an ophthalmoscope that integrates both the confocal and scanning capabilities, i.e., it allows for eye fundus imaging on a confocal plane, rejecting most of the light coming from both the anterior and posterior planes of the chosen plane. This allows for measuring the 3-D distribution of fluorescein (fluorescence) inside the eye.

We have been able to modify a recently introduced CSLO prototype from Zeiss (Carl Zeiss, Oberkochen, Germany) and to develop a new methodology to perform localized measurements of the BRB function, thus creating a map of the human BRB function [5]. Subsequent publications have demonstrated the clinical value of such methodology [15]. This instrumentation, however, had specific limitations and is not commercially available. The most important limitations are the fact that the confocal plane is continuously moving during the acquisition and that the video signal generated is an interlaced video signal. This means that each line of the image is on average 150 μm apart (along the z-axis) from the lines above and below. Another limitation is the fact that only 9 confocal planes are imaged. Still, using this instrumentation, it was possible to bring new findings to clinical research, e.g., the reversibility of the alteration on the BRB in the initial stages of DR [16].

When looking for a replacement for the Zeiss-CSLO, the established criteria was the availability, access to details and the possibility of introducing changes to the regular instrumentation. Based on these constraints, the selected instrument was the Heidelberg Retina Angiograph (HRA) (Heidelberg Engineering, Dossenheim, Germany). Changes were introduced both during the assembly procedure and thereafter by testing a set of confocal pinholes. The major differences between the Zeiss system and the Heidelberg system consists on the detector used, respectively a photomultipler tube and a photodiode, and on the fact that while the former acquires information with the confocal plane being continuously moving, the latter does not, i.e., each confocal plane is imaged without any movement along the optical axis. Section III includes more details on instrumentation characteristics.

The full procedure to compute the permeability index of the BRB can be outlined, as shown in Fig. 2.

To compute the permeability index of the BRB to fluorescein, it is necessary to compute the amount of fluorescein that crosses the BRB from the blood stream into the vitreous. This value must then be normalized by the total free fluorescein, i.e., the integral of free fluorescein concentration available in the blood stream from the time of intravenous administration to the time of data acquisition [17].

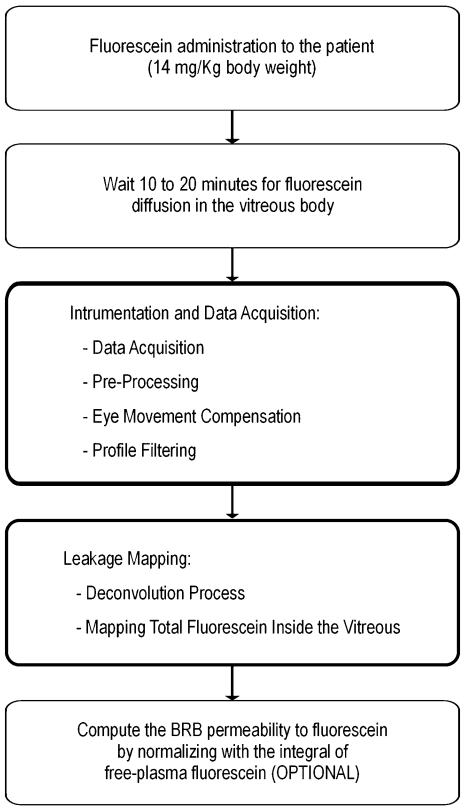

Fig. 2. Procedure overview of the entire process. The "Instrumentation and Data Acquisition" block, deals with data acquisition and all steps of data processing until data is ready for the deconvolution step. The "Leakage Mapping" block performs data deconvolution and builds the leakage map. An optional step consists on system calibration and normalization of the leakage map by the integral of free-fluorescein in the plasma, therefore computing the BRB permeability to fluorescein.

The procedure to compute the amount of fluorescein present in the vitreous is presented throughout the paper.

In Section III, the instrumentation used is presented with its technical details.

Section III-A presents the methodology used to determine the point-spread function (PSF) of the system composed by the combined optical characteristics from the instrumentation and the eye. Once this is made *in vitro* and the system is built for use in human eyes (*in vivo*), making up the final part of the optical path of the system, the apparatus for measuring the PSF will have to mimic the normal human eye in the conditions of data acquisition. To reproduce these conditions, an artificial pupil and a lens are used.

A preprocessing stage, Section III-B, specifies the validation of the gathered data.

Before deconvolving the 3-D fluorescein concentration distribution, using the established PSF, it will be mandatory to compensate for both voluntary and nonvoluntary saccadic eye movements that occur during the 1.6 s of data acquisition. Section III-C presents the methodology used in this work in order to achieve this goal.

Moreover, before the deconvolution process can take place, two major issues must be taken into account: noise on measured data and expected profile for the deconvolved signal. Noise is removed by filtering, as shown in Section III-D. The methodology to obtain the expected profile is described in Section IV-A.

For improved fundus reference, a local contrast enhancement was implemented (Section III-E).

Section IV-B presents the deconvolution process, incorporating knowledge from the previous sections, namely, the expected shape of the profile inside the vitreous.

Section IV-C helps to interpret the deconvolved profile.

Section IV-D defines the process of computing the leakage maps.

In Section V-A, the selection of representative cases is explained.

Finally, Section V-B presents the results achieved in the selected representative cases, followed by a discussion in Section V-C.

III. Instrumentation and Data Acquisition

The HRA is a confocal scanning laser ophthalmoscope system able to register the volumetric distribution of fluorescence in the human eye. It scans 32 confocal planes with 10×10, 20×20 or 30×30 degrees of amplitude. Each image-plane is made of 256×256 or 512×512 pixels. In addition, the scanning depth can be made from 0 to 7 mm with 1-mm step increments. As a result, each scan returns volumetric information made up of $256 \times 256 \times 32$ or $512 \times 512 \times 32$ voxels of one byte each.

The system uses a 488-nm wavelength argon laser source as excitation light and a barrier filter at 500 nm, which rejects the reflected light, i.e., the quantified light is the fluorescent light emitted by the fluorescein molecules excited with the argon laser source. In this way, it is possible to know the 3-D fluorescence distribution in the scanned volume.

The focus range can go from between -12–$+12$ diopters and the maximum frame rate in the FA acquisition mode is 20 image/s, i.e., a complete scan takes 1.6 s.

Two minor adjustments were introduced in the original setup: a switch allowing to choose between the original and modified acquisition modes and the confocal aperture. The former establishes a deeper scanning into the retina relative to the original configuration, while the second consists of the replacement of the original pinhole of 400 μm in diameter with a 200 μm in diameter pinhole in order to increase the confocality of the system.

The selection of the 200-μm pinhole was made based on a series of experiments using different pinhole sizes. As the pinhole size decreases, system confocality increases, but less light is collected, making it difficult to gather information from the eye fundus and restricting the acquisition time after the dye administration [18]–[22].

The protocol used in the initial studies to test the HRA for scanning the human eye fundus was as follows:.

- Acquisition mode: FA.
- Acquisition time interval: 1.6 s, beginning 10–20 min after intravenous fluorescein administration of 14 mg/Kg of body weight.
- Acquisition angle: 20° (centered on the fovea).
- Scan depth: 7 mm.
- Focus: adjusted to obtain the brightest image possible, by compensating eye power.
- Acquisition rate: 20 images/s.
- Image resolution: 256×256 pixels (8 bits/pixel).

By following this protocol, on average, $1/3$ of the planes correspond to the retina and $2/3$ are acquisitions made inside the vitreous, each plane being 225.81 μm apart from the next. The major drawback of the system is its long acquisition time, 1.6 s. Due to normal human saccadic eye movements, both voluntary and nonvoluntary, the set of planes must be aligned to build a profile along the different confocal planes (z-profile) for each location of the eye fundus image (Section III-C).

While image resolution is 256×256 pixels, due to the decreased pinhole size from the default size, with the necessary reduction of the signal-to-noise ratio (SNR), a decimation with factor 2 is made after eye movement compensation (Section III-C) and prior to the deconvolution (Section IV-B).

A. Point-Spread Function (PSF)

The acquisition of the volumetric distribution of fluorescence in the human eye depends on the combined optical characteristics from the instrumentation and the eye. For the characterization of this composed system it is necessary to determine its response to the impulse input $(\delta(t))$. A set of experiments proved that the system obeys to the homogeneity, additivity and shift invariance principles, thus being a linear-time invariant (LTI) system.

From the theory of linear systems, the output (o) of a system can be computed from both the input (i) and the system transfer function (h) by their convolution, i.e.,

$$o = h * i. \tag{1}$$

From both the derivative and the convolution theorem of the Fourier transform, the following applies:

$$o' = h * i' \tag{2}$$

with o' and i' representing the derivatives of o and i, respectively.

The application of these principles were first tested with a testing device using a 66 diopters lens to simulate the human eye power, an artificial pupil with 8 mm in diameter, so as to mimic the human pupil dilation in the conditions of the examination, and a set of *cuvettes* filled with different fluorescein concentrations.

With the aforementioned setup, the *cuvette*-lens distance was adjusted so that a step input-function was produced, i.e., in one extreme of the scanning depth, the focal plane is placed outside the *cuvette*, while in the other extreme it is inside the *cuvette*, thus measuring the fluorescence produced by the fluorescein.

Using xyz coordinates with z representing the z-axis, i.e., the optical axis that is normal to each image plane, xy, and making i the *Heaviside* unit step function, $H(z)$, its derivative, i', is the impulse function $\delta(z)$, while the derivative of the output, o', represents the PSF of the system.

The best-fit function found for the PSF is a *Lorentzian* profile with the equation:

$$\text{fluorescence}(z) = \frac{2Aw}{\pi(w^2 + 4(z - z_c)^2)} \tag{3}$$

with w being the full-width at half-maximum (FWHM), A the area under the curve from $z = -\infty$ to $z = \infty$, and z_c the abscissa where the maximum $(2A/\pi w)$ occurs.

For the determination of the PSF, a set of *cuvettes* filled with different fluorescein concentrations were used and scans were taken using different scan depths (5, 6, and 7 mm). For each scan, several z-profiles were considered by sampling different positions in the image plane. Besides the natural differences in the z_c parameter, as *cuvettes* have planar surfaces, no differences were found for the A or w parameters, thus showing the system space invariance.

The fitting procedure was done using both the derivative (finite differences) of the output and the Lorentzian and the output and the antiderivative of the Lorentzian (4). Sample spacing of data ranged from 161.29 μm (5-mm scan depth) to 225.81 μm for 7-mm scan depth (193.55 μm for 6-mm scan depth).

$$\int \frac{2Aw}{\pi(w^2 + 4(z - z_c)^2)}\, dz = \frac{A}{\pi} \arctan \frac{2(z - z_c)}{w} \tag{4}$$

The determined FWHM is 1287 μm, although a correction factor of 0.75 proved to provide better results in the deconvolution process (Section IV-B).

The plot in Fig. 3 illustrates the PSF by showing the z-profile of a scan of a thin fluorescent sample. The measured FWHM of this profile is 1253.2 μm.

The knowledge of the PSF can then be used to deconvolve the output produced by a scan, thus allowing to recover the fluorescein distribution in the human eye and to compute the total fluorescein that crossed the BRB and entered the vitreous.

B. Preprocessing

The preprocessing stage consists of importing data and verifying their values obey to predetermined conditions.

Initially, a z-axis profile of the average fluorescence intensity for each confocal plane is estimated. This profile is then analyzed with regard to its shape, i.e., checking for flat scans (5), the number of local maxima and the SNR.

The SNR is estimated by (6)

$$|\mu(z_i) - \mu(z_{i-1})| \leq 2, \quad \forall i \in \{2, \ldots, 32\} \tag{5}$$

$$\text{SNR} = 10 \log_{10} \frac{\sigma^2_{\text{signal}}}{\sigma^2_{\text{noise}}} \tag{6}$$

where $\mu(z_i)$ is the mean fluorescence of plane (i) and σ^2_{signal} and σ^2_{noise} are the *variance* of the confocal plane with higher average intensity and lower average intensity along the z-axis, respectively.

Only nonflat scans having a single local maximum and with a $\text{SNR} \geq 9$ dB are considered for processing.

It should be noted that the SNR expression (6) may indicate erroneous values for artificial systems similar to the system described in Section III-A (scanning *cuvettes*). Scanning such devices, the acquisitions of confocal planes inside the *cuvette*, with high values of concentration, will show lower *variances* compared to acquisitions of confocal planes outside the *cuvette*. Nevertheless, for practical use on human eyes, it represents a fairly good and useful indicator of SNR.

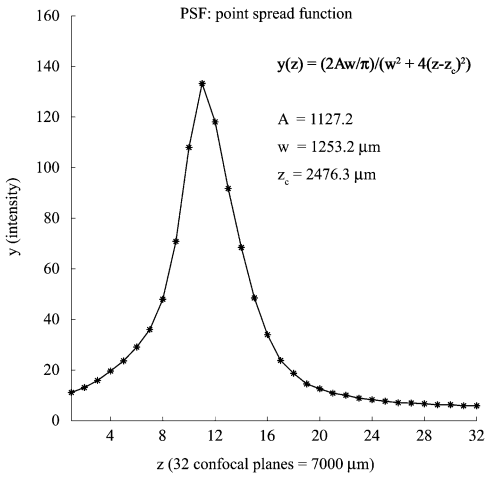

Fig. 3. Profile obtained by scanning a thin fluorescent sample, thus representing the PSF of the system. The FWHM of this profile is 1253.2 μm, computed by fitting a Lorentzian function to data. Fitted parameters are $A = 1127.2, w = 1253.2\ \mu$m, and $z_c = 2476.3\ \mu$m.

C. Eye Movement Compensation

As stated above, due to saccadic eye movements, it is necessary to compensate for their movements. A discrete *Phase Correlation* function is used [23], [24] which is based on the shift property of the Fourier transform, i.e., if $f(x)$ has the Fourier transform $F(u)$, then $f(x - a)$ has the Fourier transform $e^{-j2\pi au}F(u)$.

Given two images, $g_1(x, y)$ and $g_2(x, y)$, their Fourier transform can be written using the *Euler* notation as

$$G_1(u, v) = \Im\{g_1(x, y)\} = |G_1(u, v)| \cdot e^{j\phi_1(u,v)} \tag{7}$$

$$G_2(u, v) = \Im\{g_2(x, y)\} = |G_2(u, v)| \cdot e^{j\phi_2(u,v)}. \tag{8}$$

Their product is

$$G_1(u, v)G_2^*(u, v) = |G_1(u, v)||G_2(u, v)| \cdot e^{j(\phi_1(u,v) - \phi_2(u,v))} \tag{9}$$

from which

$$e^{j\Phi(u,v)} = \frac{G_1(u, v)G_2^*(u, v)}{|G_1(u, v)G_2^*(u, v)|}. \tag{10}$$

Finally

$$d(x, y) = \Im^{-1}\left\{e^{j\Phi(u,v)}\right\} \tag{11}$$

where $\Phi(u, v) = \phi_1(u, v) - \phi_2(u, v)$ represents the phase array.

The maximum of $d(x, y)$ occurring at (x_d, y_d) gives the displacement in both x and y directions of x_d and y_d, respectively.

This automatic procedure is applied to the whole volume of information, thus compensating for the saccadic eye movements along the acquisition time, i.e., along the confocal planes. The forehead is pressed tightly against the head rest and the chin against the chin rest, thus avoiding eye movements along the

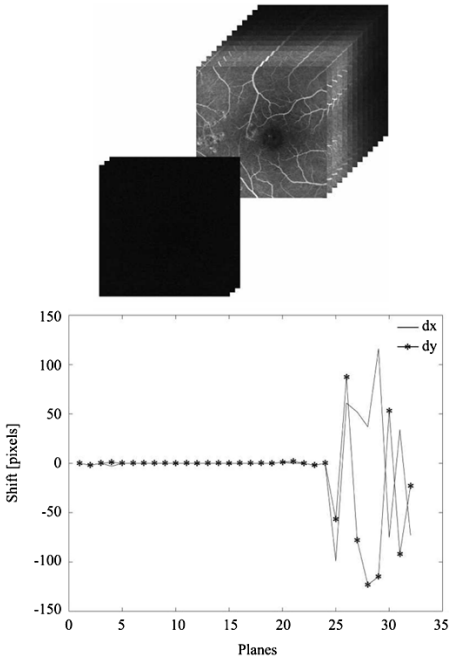

Fig. 4. Volumetric information made of up 32 confocal planes (top) and the respective computed displacements between planes (bottom). Positive shifts on the x- (dx) and y-axis (dy), correspond to shifts to the right and up, respectively.

z-axis. Nevertheless, if such movements occur, they will produce local maxima in the fluorescence profiles along the z-axis and are, thus, detected in the preprocessing stage (Section III-B).

Fig. 4 represents both a set of confocal planes, at the top, and the corresponding displacements plotted as a line-graph, at the bottom.

Due to the fast decrease of image intensity along the confocal planes as we move away from the retina-vitreous interface, the SNR decreases and as a result, the computed displacement between planes may increase due to noise. The limit established to consider a plane as being part of the aligned volume is based upon both the displacement between planes and the average intensity level of the whole image plane. Therefore, even though all scans have 32 confocal planes, not all of them are considered for further processing. The minimum number of confocal planes considered for processing a given scan is 17 confocal planes. This number proves to be enough for processing, while simultaneously giving access to more than 90% of the total patient scans, which is an important parameter.

It is now possible to build a z-profile of the fluorescence distribution along the confocal planes for each pixel of the eye fundus.

The fact that planes belonging to the vitreous are being aligned is possible considering the large FWHM and the fact that the method used does not rely on landmarks, which would be difficult to extract from the mentioned planes. Moreover, not using the whole set of confocal planes does not represent a drawback as for the time allowed for fluorescein diffusion inside the vitreous, i.e., the diffusion time from intravenous fluorescein administration to the time of scan, fluorescein does not go further than 1.5 mm from the retina-vitreous interface. Therefore, even considering the worst scenario, i.e., only 10 out of 17 planes being measurements in the vitreous, this would represent more than a 2-mm scan inside the vitreous, thereby covering the volume of interest.

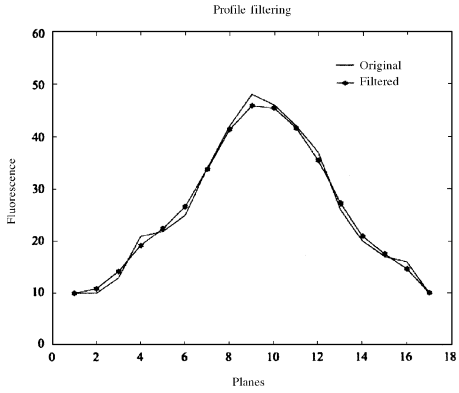

Fig. 5. Profile preprocessing: effect of low-pass filtering of the original profile. Solid-line only and solid-line plus dots represent, respectively, the original and filtered profiles.

D. Profile Filtering

After correcting for saccadic eye movements, a fluorescence profile can be built for any position on the eye fundus in the scanned area.

A finite-impulse response (FIR) low-pass filter was determined that permits the removal of some of the high frequency components that, given the PSF already determined, cannot correspond to real fluorescence levels but to a sum of the former, with noise, while capturing the global shape of the measured profile.

The filter that proved to produce better results is a fourth-order FIR filter with a relative cutoff frequency of 0.6.

Fig. 5 shows both the original and filtered signals, the latter being the smoother of the two, in a typical profile, where the x-axis represents the position of the confocal plane and the y-axis represents the intensity of the fluorescence level.

E. Computed Fundus Image

In order to improve the fundus image, and only for reference purposes, a local contrast enhancement (LCE) algorithm is used.

Given the small pinhole size and the fact that the sensor is a photodiode and not a photomultiplier tube (PMT), the original images of eyes from older people and/or eyes with media opacities present characteristically low levels.

Based on the algorithm presented in [25], each value of intensity $f(x, y)$ is replaced by g, given by

$$g = \mathrm{Max}_{\mathrm{level}} \frac{G(f) - G(f_{\min})}{G(f_{\max}) - G(f_{\min})} \tag{12}$$

where

$$G(f) = \left[1 + e^{\frac{(\langle f \rangle_w - f)}{\sigma_w}}\right]^{-1} \tag{13}$$

with $\mathrm{Max}_{\mathrm{level}}$ the maximum value for the image intensity, $\langle f \rangle_w$ being the mean value for a subimage W centered on (x, y) with dimensions $N \times N$ and σ_w being the standard deviation in W. For details see [25]. Typical used values for $\mathrm{Max}_{\mathrm{level}}$ and N are 255 and 31, respectively. The N value was chosen based on a

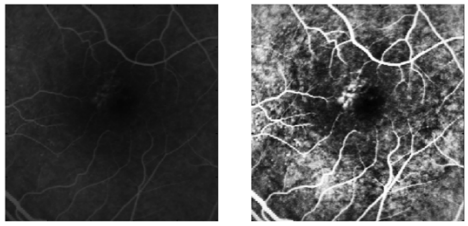

Fig. 6. Local contrast enhancement effect. Left: original fundus image. Right: local contrast enhanced fundus image, showing a more contrasted fundus image (for fundus reference purposes only).

subjective evaluation made by the final users and corresponds to their perception of the best fluorescein angiographic image.

Since the size of the images acquired with the HRA are small, 256×256 pixels maximum, by following the protocol and due to the alignment, and to overcome the effect of the borders of the image, instead of considering the outer values as null, a larger image is created by duplicating strips of width $(N-1)/2$, N is odd, along the edges of the image, i.e., the image grows in size from $A \times B$ to $(A + 2 \times (N-1)/2) \times (B + 2 \times (N-1)/2)$ pixels.

The result is shown on Fig. 6.

The fundus image on the right is the result of applying the LCE method to the fundus image as shown on the left. The increase in details found is obvious.

IV. Leakage Mapping

A. Diffusion Physical Model

Even knowing that once inside the vitreous the movement of fluorescein is due to a simple diffusion process, i.e., depends on the gradient of concentration, close to the retina-vitreous interface and for the time range of interest, it is necessary to establish the expected profile in order to include its model in the deconvolution process (Section IV-B). The expected profile of distribution of fluorescein necessarily depends on the time after fluorescein administration. After a period of several hours, the level of fluorescein in the blood stream is lower than inside the vitreous. At that time, the fluorescein will be diffusing in the opposite direction. This fact clearly demonstrates the need to establish the distribution profile for the time range of interest—10–20 min.

The process of diffusion of fluorescein from the blood stream into the vitreous can be modeled as a two-compartment model, compartments A and B and a barrier in between.

The equation defining the diffusion process from compartment A to compartment B, i.e., through the barrier, is

$$J = P\Delta C \tag{14}$$

where J is the current density, P is the permeability of the barrier to fluorescein, and ΔC is the difference in concentration between the two compartments.

Inside the vitreous, the fluorescein movement modeled by a one-dimensional and isotropic diffusion process, is given by (*first Fick's law*)

$$F = -D\frac{\partial C}{\partial x} \tag{15}$$

where F is the rate of transfer/unit area, C is the fluorescein concentration in the vitreous, and D is the diffusion coefficient.

The fundamental differential equation of diffusion is derived from the above equation resulting in (*second Fick's law*)

$$\frac{\partial C}{\partial t} = D\frac{\partial^2 C}{\partial x^2}. \tag{16}$$

Considering, hypothetically, the fluorescein concentration as a constant in the blood stream, the deterministic solution is given by

$$C(x,t) = C_0 \mathtt{erfc}\frac{x}{2\sqrt{Dt}} \tag{17}$$

where $\mathtt{erfc}(z) = 1 - \mathtt{erf}(z)$ [26].

Although this expression may be a close representation for the first minutes after fluorescein administration, we do not consider it for practical use. Moreover, the fluorescein concentration in the plasma $(C_p(t))$ cannot be considered constant.

In [22] it can be seen that the fluorescein concentration in the plasma $(C_p(t))$ is given by

$$C_p(t) = K(10^{-1.17t} + 0.115 \times 10^{-0.34t} + 0.025 \times 10^{-0.044t}) \tag{18}$$

where K depends on the administered dose and absorption, and t is the time after the intravenous fluorescein administration, in hours. This expression is similar to the one found in [27] besides an extra term in the sum.

Although (17) may be a close representation for a short period of time after intravenous fluorescein administration, it does not express the reality of the time range of interest ($t \in [10, 20]$ min) where the data acquisition takes place. According to (18), the fluorescein concentration in the plasma decreases to 76.4% and to 52.0%, 10 and 20 min after intravenous fluorescein administration, respectively.

We followed a different approach by searching for a solution for the diffusion process expressed by (14)–(16). A finite element method was used in order to solve (16) so as to find the curve of the fluorescein concentration inside the vitreous for the time range of interest.

Our model assumes a homogeneous BRB without active transport being involved in the movement of fluorescein and an intact vitreous gel. Therefore, the diffusion coefficient (D) and permeability (P) are considered as constants [17], [28]–[31]. Several simulations were run using different values for D and P. For the simulation shown, the values of D and P used are 9.5×10^{-6} cm^2·s^{-1} and 22×10^{-7} cm·s^{-1}, respectively. For D, there are different values published in the literature, 1×10^{-5} cm^2·s^{-1}, 8×10^{-4} cm^2·min^{-1}, and 6×10^{-6} cm^2·s^{-1}, respectively in [17], [22], and [28], while for P, the value was chosen in the range established in [5].

The simulation ran for the time period of interest, i.e., $t \in [0, 20]$ min, although only in a small number of patients it is possible to obtain clear images for $t > 16$ min after the dye administration.

The results of the simulation for 10, 15, and 20 min after intravenous fluorescein administration and in the conditions stated above are shown in Fig. 7.

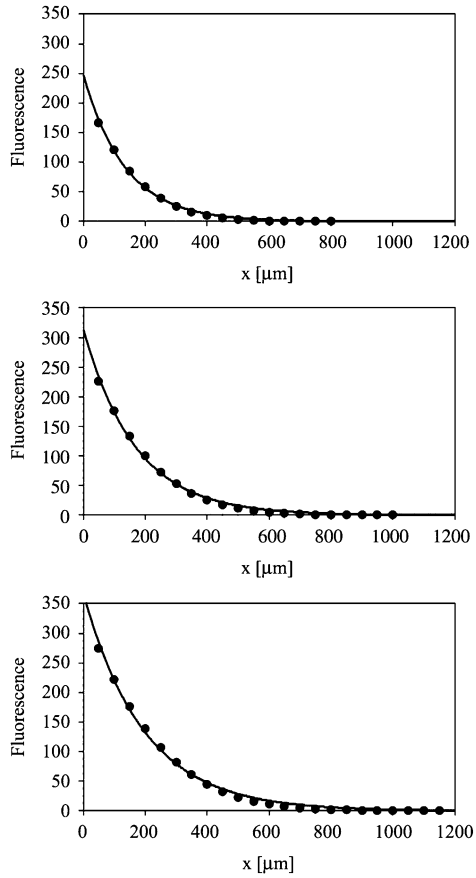

Fig. 7. Simulation showing the fluorescein distribution in the vitreous for 10, 15, and 20 min after intravenous fluorescein administration, top, middle, and bottom, respectively. The x-axis shows the distance to the retina $(x = 0)$ in microns. Dots shows computed values of fluorescein and solid-lines shows the respective monoexponential fits. It is possible to see the income of fluorescein over time as well as the diffusion occurring in the vitreous.

As illustrated in Fig. 7, the penetration of fluorescein into the vitreous over time is clear and the monoexponential profile as a function of the distance to the BRB interface (x-axis, [μm]) for the time period of interest, represents a reasonable approximation. Therefore, the monoexponential model may be incorporated into the deconvolution process.

Data points are shown as black circles and best-fit exponentials are shown as black solid-lines, whose expressions are

$$y(x) = 246.9 \times e^{-0.0074x}, \quad t = 10\,\text{min} \tag{19}$$

$$y(x) = 313.1 \times e^{-0.0059x}, \quad t = 15\,\text{min} \tag{20}$$

$$y(x) = 366.0 \times e^{-0.0051x}, \quad t = 20\,\text{min}. \tag{21}$$

A close look into the fitting allows to verify that the fitting is not perfect and changes over the time, showing that the monoexponential fit, while reasonable, does not convey all the details of the original profile. Nevertheless, this degree of accuracy is sure-enough for the purposes of current work.

This simulation/fitting procedure establishes that the expected curve for the distribution of fluorescein in the human vitreous can be modeled by a monoexponential whose parameters can be simply computed from data for the time range of interest for the current application. A set of simulations using different values for P and D support this statement. A tail of a Gaussian also fits the curve but needs an optimization algorithm to find its parameters. This extra effort is worthless. Moreover, the use of a simpler exponential fit allows for its usage in the deconvolution process, described later, thus looking for a solution that obeys the physical model of the diffusion.

B. Deconvolution Process

The fluorescence profile does not represent by itself, the real fluorescence distribution, but the result of its convolution with the PSF. Therefore, it is mandatory to perform the deconvolution of each profile in order to recover the real fluorescence distribution.

Although several methodologies exist for performing deconvolutions, the present application has several peculiarities.

The first is the fact that a limited number of samples exist for the fluorescence profile, 32 maximum, but most of the time, a smaller number of samples is used, as stated above.

Another peculiarity is the fact that there are no negative concentrations, i.e., during the deconvolution process it is necessary to guarantee that all values are nonnegative. Moreover, since the shape of the fluorescein concentration curve in the vitreous is now established, this information is brought into the deconvolution process to produce a final result in accordance with the established physical model. To overcome these facts, the following procedural approach is taken.

- A PSF is created from the parameters found when determining the system PSF with samples 50 μm apart.
- The real (measured) profile is replaced with its filtered version (Section III-D), thus attenuating the noise effects, as those seen in Fig. 5, abscissa planes 12 and 16.
- An iterative process is used that:

1) starts by using a string of zeros as a hypothetic input. Samples are 50 μm apart, as in the PSF;
2) computes the hypothetic output by computing the convolution of this input with the PSF;
3) interpolates this output signal by means of a spline function at the real sampled profile locations (161.29, 193.55, and 225.81 μm apart, for 5-, 6-, and 7-mm scan depths, respectively);
4) computes the difference between the filtered and interpolated profiles;
5) linearly interpolates the difference profile at the location of the hypothetic input;
6) updates the hypothetic input by a fraction of the error (λ);
7) checks for nonpositive values of concentration;
8) finds the maximum of the updated hypothetic input, that is considered the retina-vitreous interface;
9) puts the focus on this location by updating the value of the hypothetic input with half of the above updated value, i.e., at this location 1.5λ is used instead of λ;
10) from this location into the vitreous side, it is guaranteed that the signal is not increasing by making higher values than the previous ones equal to them;
11) an exponential is fitted to this data;

12) this data is then replaced by the values resulting from the evaluation of the fitted exponential function;
13) the process repeats steps 2)–12) until the maximum number of iterations is reached or the error signal is lower than 5% of the filtered profile;

This procedure guarantees the definition of the location of the highest peak of the deconvolved profile (retina-vitreous interface) in association with the expected diffusion profile of the fluorescence distribution in the vitreous.

For mapping the BRB for all scanned areas, the deconvolution process (Section IV-B) must be repeated for each position of the eye fundus image. The results of this mapping procedure are presented in Section V.

C. Retina Physical Model

The scanned volume of the human eye fundus, considering the 7-mm scan depth established in the protocol, means that there are confocal planes measured in the vitreous, in the retina, and in the choroid.

Fig. 8 shows that the deconvolved profile does not consist of a single impulse representing the retina, but a string of impulses. The location of the retina-vitreous is herewith considered to be the location of the highest peak of the deconvolved profile, as stated in Section IV-B. The string of impulses from this location to the right represents readings belonging to the vitreous, while the string of impulses to the left represents readings in the retina. The several layers of the retina and their vascularization can be seen in [32], which explains the string of impulses.

D. Mapping Total Fluorescein Inside the Vitreous

The amount of fluorescein present in the vitreous, in front of the (x, y) coordinates of the eye fundus, is given by

$$\mathrm{LU}(x,y) = \int_{z_0}^{z_1} C_{\mathrm{vitreous}}(x,y,z)\, dz \tag{22}$$

where $C_{\mathrm{vitreous}}(x,y,z)$ is the fluorescence intensity inside the vitreous and LU stands for *Leakage Units*. Typical used values for z_0 and z_1 are, respectively, 100 μm and 1000 μm, with $z = 0$ being the location of the retina-vitreous interface.

The diffusion physical model, established in Section IV-A, allows knowing the expression for $C_{\mathrm{vitreous}}(x,y,z)$, it being of the form:

$$C_{\mathrm{vitreous}}(x,y,z) = k(x,y)e^{-\alpha(x,y)z} \tag{23}$$

with $k(x,y) \geq 0$ and $\alpha(x,y) > 0, \forall x \in \{1 \ldots M\}, y \in \{1 \ldots N\}$, and $M \times N$ the size of the fundus image. The values for $k(x,y)$ and $\alpha(x,y)$ are computed by the procedure for the deconvolution process described in Section IV-B.

The leakage maps are therefore given by

$$\mathrm{LU}(x,y) = \frac{k(x,y)}{\alpha(x,y)}\left[e^{-\alpha(x,y)z_0} - e^{-\alpha(x,y)z_1}\right] \tag{24}$$

where $k(x,y)$ and $\alpha(x,y)$ are computed fitting an exponential to the profile of distribution of fluorescence inside the vitreous (deconvolved profile) in front of the (x,y) coordinates of the fundus image.

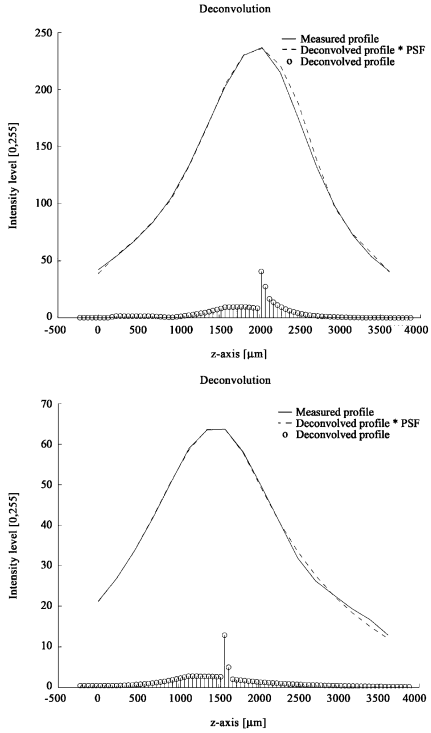

Fig. 8. The deconvolution process. Solid-lines represent the filtered version of the measured profiles, while stem plots (vertical lines terminated with a circle) represent the real fluorescence distribution which is obtained by the deconvolution process. Dash-lines represent the theoretical output computed based on the deconvolved profile and on the PSF of the system. The location of the retina-vitreous interface is considered to be given by the location of the highest value of the deconvolved profile. A marked income of fluorescein into the vitreous (part of the deconvolved profile to the right of its highest value) versus a residual measure (no leakage) can be seen on the top and bottom plots, respectively. Please note the difference in the intensity scale.

V. Experiments and Results

A. Clinical Testing Method

Human clinical situations representing specific testing situations, already demonstrated in previous studies [5], were chosen to test the novel instrumentation and methodology.

The chosen clinical set is as follows:

- *Normal, control situation of the human eye:* three healthy eyes from people of different ages.
- *Eyes having abnormal fundus fluorescence but no alteration of the BRB:* three eyes with drusen of the fundus.
- *Eyes which present alterations of the BRB:* three eyes with nonproliferative diabetic retinopathy.
- *Eyes presenting a well-defined localized alteration of the BRB:* two eyes submitted to focal argon laser photocoagulation.

B. Results

The application of this methodology to different situations of altered BRB permeability is shown in Fig. 9(a)–(d), where the fundus images are shown on the left and the respective leakage maps computed by (24) are shown on the right. These four examples correspond to well demonstrated different situations of the BRB and allow, therefore, to test the performance of the system in typical cases. Moreover, the system was tested in a

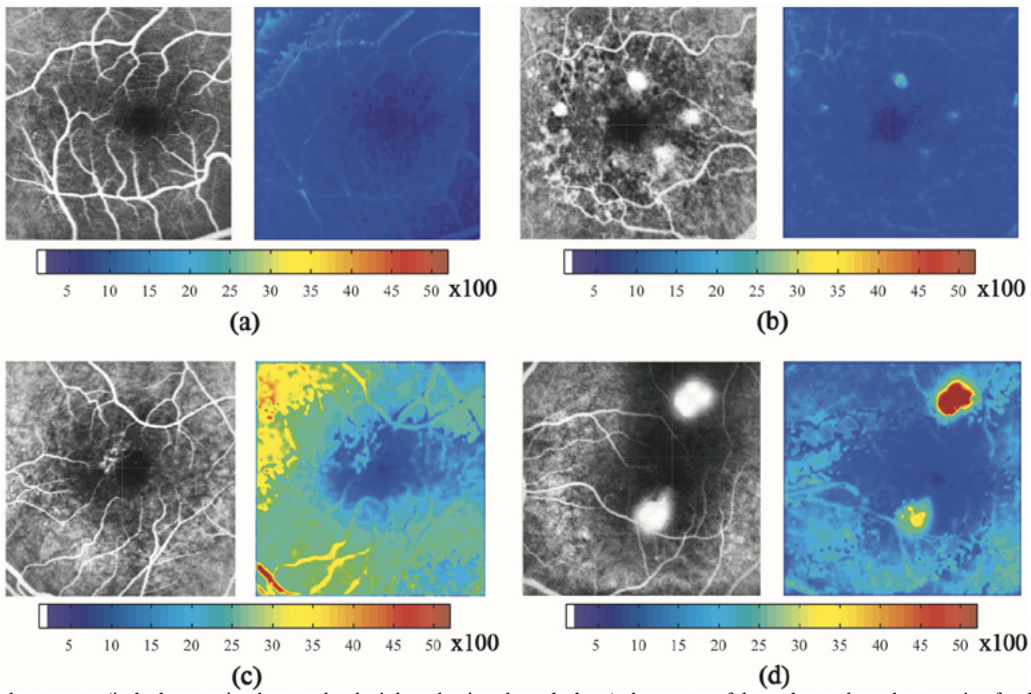

Fig. 9. Results. Leakage maps (in leakage units that can be deciphered using the colorbars) shown on a false color-code and respective fundus references (local contrast enhanced fluorescein angiographies). Top row: two cases with intact BRB, a healthy eye (on the left), and a eye with small drusen (on the right), a left eye from a 35 years-old woman and a right eye from a 76 years-old woman, respectively. Bottom row (left): eye with nonproliferative diabetic retinopathy from a 62 years-old woman (left eye). Bottom row (right): eye three days after laser photocoagulation from a 46 years-old diabetic woman (left eye).

series of eyes from type 2 diabetic patients with results that correspond to the expected evolution of the disease. These data will be the subject of future publications in medical journals.

It must be taken into account that the leakage maps, shown in color-coded fashion, represent leakage as defined by (22), i.e., the integral from z_0 to z_1, being $z = 0$ the position of the maximum found for each deconvolved profile. Moreover, each profile represents the fluorescence intensity distribution along the optical axis (z-axis) as no conversion into equivalent concentrations of fluorescein was performed.

In eyes that have an intact BRB, i.e., healthy eyes and eyes with small drusen it becomes clear that the measurements obtained with this system are independent of the intensity levels and that the system is really measuring only fluorescence inside the vitreous and not inside the retinal vasculature or in the retina. The fact that the leakage map is not completely uniform, showing spotty amounts of fluorescein leakage in the neighborhood of some retinal vessels is probably due to the fact that even in healthy retinas there is some degree of leakage, as already stated in Section II.

The eyes with multiple small drusen demonstrate particularly well that autofluorescence of the drusen material is not measured by our system as leakage.

The eyes with nonproliferative diabetic retinopathy showed clearly increased amounts of fluorescein in the vitreous in patterns similar to the ones represented in Fig. 9(c).

Focal photocoagulation induces a localized breakdown of the BRB. The eyes examined three days after laser photocoagulation showed well the localized increase in fluorescence in the vitreous in the photocoagulated areas.

C. Discussion

A computational application was developed under the software development tool *Matlab R12* [33] allowing to produce these first results. These results are in agreement with our previous knowledge, based on a previously developed prototype and with the results achieved with it [5], [15], and [16]. Since no *gold standard* exists it was not possible to correlate the achieved results with any current clinical standard.

Future developments of this methodology for clinical application will take into account the necessary correction procedures and calibration into equivalent of fluorescein concentration (eq. ng/ml).

Besides the calibration, the full procedure is automatic and supported by the developed computational application. Depending on the volumetric alignment (due to saccadic eye movements during acquisition), a single scan takes between 5 and 8 min of processing time on a Pentium IV 1.7-MHz computer. Also, the developed application can be run either in the single or batch processing mode. The batch processing mode is suitable for overnight processing of a series of scans enclosed in a given directory and/or subdirectories.

The above mentioned calibration procedure allows to convert fluorescence intensity into equivalents of fluorescein concentration (eq. ng/ml) and consists of scanning a *cuvette* filled with a known concentration of fluorescein and therefore to compute the conversion factor. This step allows to quantify the fluorescein inside the vitreous and to obtain maps of leakage, in mm·ng/ml units, according to (22). This makes possible to compute the BRB permeability as in [5], i.e., in cm·s^{-1}.

On the other hand, to compensate for changes in lens opacities in one eye followed over time, our proposal is to use one of the large vessels close to the optic disk as a reference under well-controlled conditions, e.g., after a defined fluorescein administration and at a specific time after administration or, alternatively, correcting for fluorescein plasma concentration for the time of scan.

In order to convert between fluorescence levels into equivalents of fluorescein concentration, it is necessary to calibrate the

system using a cuvette filled with a known concentration of fluorescein. In this way, it is possible to have values indicative of the distribution of fluorescein concentration (e.g., in eq. ng/ml) inside the human vitreous. Such step would allow comparison with values of BRB permeability to fluorescein in [5] or values obtained using vitreous fluorometry.

The current clinical routine of FA does not provide quantitative evaluation of fluorescein leakage. Therefore, our application, using off-the-shelf computers, compares favorably to FA. Moreover, the *batch* processing option allows its use in large clinical trials.

Although it is possible to represent leakage maps as 3-D maps, it was considered that they would be better represented as two–dimensional maps, thus making it easier to establish correlations to the fundus reference. The developed software also allows to export leakage maps as a matrix of values. These value can then be further processed with any other software package in order to compute several parameters of interest, e.g., average values, skewness, kurtosis, etc.

VI. Comments and Conclusion

In this paper, we have presented a method for computing fluorescein leakage from the retinal circulation into the vitreous of human eye *in vivo*. The focus was kept on the technique for computing the amount of fluorescein that crossed the BRB and penetrated into the vitreous. Arbitrary units, named *leakage units*, were used since fluorescence measurements were not converted to equivalent fluorescein concentration.

The presented methodology can also be used to compute the BRB permeability to fluorescein by converting fluorescence levels to equivalent fluorescein concentration and normalizing the computed amount of fluorescein inside the vitreous by the integral of free-plasma fluorescein, as mentioned in Section II. Currently, it is thought that it would be more important to discriminate between different leaking sites within the same eye than having an absolute value of permeability. Therefore, *leakage units* will be enough, even for follow-up, as the amount of injected dye is normalized by body weight. In this case, normalization for different gains can be easily achieved by using the fluorescence level of a large vessel close to the optic disc head, which is both faster and easier than the use of a *cuvette* filled with a known concentration of fluorescein, as mentioned in the text.

The method described here represents an important step in the assessment of the BRB function, as it allows the mapping of retinal fluorescein leakage into the human vitreous in relation to the retinal morphology. Moreover, the method described is based on a commercially available CSLO instrumentation, allowing the methodology to be applied in different centers of medical research, since the applied changes to the basic instrumentation do not represent a major challenge. The application of this methodology opens new perspectives for our understanding of retinal vascular disease, especially diabetic retinopathy. It is now possible to follow the alterations of the BRB in the human retina since their initial stages and evaluate their natural history, with regard to location, reversibility and relationship with other natural or systemic alterations. It represents a quantitative evaluation of the leakage compared to the qualitative assessment made based on the clinical experience of the FA grader in detecting and quantifying diabetic retinopathy, as well as identifying the leaking sites. A particularly useful application of this methodology will be the assessment of drug effects for clinical trials as well as early diagnosis, as changes in the BRB are detected and identified before they are seen in regular angiography.

Acknowledgment

The authors would like to thank Heidelberg Engineering and especially Dr. G. Zinser for their support in introducing the switch to select between the regular mode and the special fluorescein angiographic-mode for leakage measurement, as well as their support in making available a set of confocal apertures for testing. They would also like to thank the technicians involved in dealing with patients and data collection, Dr. C. Lobo for her comments, and E. Longo for her help in proofreading this paper.

References

[1] H. King, "The epidemic of NIDDM: An epidemiological perspective," *Int. Diab. Fed. Bull.*, vol. 40, no. 2, pp. 10–12, 1995.

[2] L. P. Aiello, T. W. Gardner, G. L. King, G. Blankenship, J. D. Cavallerano, F. L. Ferris III, and R. Klein, "Diabetic retinopathy (technical review)," *Diabetes Care*, vol. 21, no. 1, pp. 143–156, 1998.

[3] A. Green, N. C. Hirsch, and S. K. Pramming, "The changing world demography of type 2 diabetes," *Diabetes Metab. Res. Rev.*, vol. 19, pp. 3–7, 2003.

[4] R. T. Smith, C. J. Koester, and C. J. Campbell, "Vitreous fluorophotometer data analysis by deconvolution," *Invest. Ophthalmol. Vis. Sci.*, vol. 27, pp. 406–414, 1986.

[5] C. Lobo, R. Bernardes, F. Santos, and J. G. Cunha-Vaz, "Mapping retinal fluorescein leakage with confocal scanning laser fluorometry of the human vitreous," *Arch. Ophthalmol.*, vol. 117, pp. 631–637, 1999.

[6] F. Docchio and L. Biancardi, "Euroeye Atlas of Ocular Fluorophores," European Union Concerted Action Biomedical Engineering Ocular Fluorometry, Coimbra, Portugal, Tech. Rep., 1995.

[7] E. M. Kohner and A. R. Alderson, "Vitreous fluorophotometry," *Trans. Ophthal. Soc. U.K.*, vol. 101, pp. 446–449, 1981.

[8] J. G. Cunha-Vaz, J. R. Faria de Abreu, A. J. Campos, and G. M. Figo, "Early breakdown of the blood-retinal barrier in diabetes," *Br. J. Ophthalmol.*, vol. 59, pp. 649–656, 1975.

[9] S. R. Waltman, C. Oestrich, T. Krupin, S. Hanish, S. Ratzan, J. Santiago, and C. Kilo, "Quantitative vitreous fluorophotometry: A sensitive technique for measuring early breakdown of the blood-retinal barrier in young diabetic patients," *Diabetes*, vol. 27, pp. 85–87, 1978.

[10] S. R. Waltman, T. Krupin, C. Kilo, and B. Becker, "Vitreous fluorophotometry in adult-onset diabetes mellitus," *Am. J. Ophthalmol.*, vol. 88, pp. 342–345, 1979.

[11] J. G. Cunha-Vaz, "A brief historical note on ocular fluorophotometry," *Grafe's Arch. Clin. Exp. Ophthalmol.*, vol. 222, 1985.

[12] R. C. Zeimer, N. P. Blair, and J. G. Cunha-Vaz, "Vitreous fluorophotometry for clinical research. I. Description and evaluation of a new fluorophotometer," *Arch. Ophthalmol.*, vol. 101, pp. 1753–1756, 1983.

[13] ——, "Vitreous flurophotometry for clinical research. II. Method of data aquisition and processing," *Arch. Ophthalmol.*, vol. 101, pp. 1757–1761, 1983.

[14] R. C. Zeimer, N. P. Blair, M. M. Rusin, and J. G. Cunha-Vaz, "The performance of a new commercial ocular fluorophotometer in the clinical environment," *Graefe's Arch. Clin. Exp. Ophthalmol.*, vol. 222, pp. 222–223, 1985.

[15] C. Lobo, R. Bernardes, and J. G. Cunha-Vaz, "Alterations of the blood-retinal barrier and retinal thickness in preclinical retinopathy in subjects with type 2 diabetes," *Arch. Ophthalmol.*, vol. 118, pp. 1364–1369, 2000.

[16] C. Lobo, R. Bernardes, J. R. F. de Abreu, and J. G. Cunha-Vaz, "One-year follow-up of blood-retinal barrier and retinal thickness alterations in patients with type 2 diabetes mellitus and mild nonproliferative retinopathy," *Arch. Ophthalmol.*, vol. 119, pp. 1469–1474, 2001.

[17] P. S. Chahal, P. J. Chowienczyk, and E. M. Kohner, "Measurement of blood-retinal barrier permeability: A reproducibility study in normal eyes," *Invest. Ophthalmol. Vis. Sci.*, vol. 26, pp. 977–982, 1985.

[18] A. G. Palestine and R. F. Brubaker, "Pharmacokinetics of fluorescein in the vitreous," *Invest. Ophthalmol. Vis. Sci.*, vol. 21, pp. 524–549, 1981.
[19] B. Krogsaa, H. Lund-Andersen, J. Mehlsen, L. Sestoft, and J. Larsen, "The blood-retinal barrier permeability in diabetic patients," *Acta Ophthalmologica*, vol. 59, pp. 689–694, 1981.
[20] H. Lund-Andersen, B. Krogsaa, and P. K. Jensen, "Fluorescein in human plasma *in vivo*," *Acta Ophthalmologica*, vol. 60, pp. 709–716, 1982.
[21] M. C. Mota, E. Leite, B. A. Fernandes, M. G. Abreu, and J. G. Cunha-Vaz, "Cinética da fluoresceína no plasma," *Exp. Ophthalmol.*, vol. 8, pp. 8–12, 1982.
[22] R. C. Zeimer, N. P. Blair, and J. G. Cunha-Vaz, "Pharmocokinetic interpretation of vitreous fluorophotometry," *Invest. Ophthalmol. Vis. Sci.*, vol. 24, pp. 1374–1381, 1983.
[23] J. J. Pearson, D. C. Hines, S. Golosman, and C. D. Kuglin, "Video-rate image correlation processor," *Proc. SPIE*, vol. 119, pp. 197–205, 1977.
[24] Q. X. Wu, P. J. Bones, and R. H. T. Bates, "Translational motion compensation for coronary angiogram sequences," *IEEE Trans. Med. Imag.*, vol. 8, no. 3, pp. 276–282, Sep. 1989.
[25] R. S. B. Newsom, C. Sinthanayotin, J. Boyce, A. G. Casswell, and T. H. Williamson, "Clinical evaluation of 'local contrast enhancement' for oral fluorescein angiograms," *Eye*, vol. 14, pp. 318–323, 2000.
[26] J. Crank, *The Mathematics of Diffusion*, London: Oxford University Press, 1970, pp. 9–25.
[27] L. L. Knudsen, T. Olsen, and F. Nielsen-Kudsk, "Fluorescein anf fluorescein glucuronide in plasma," *Acta Ophthalmologica*, vol. 70, pp. 447–453, 1992.
[28] P. Dalgaard, V. A. Barker, and H. Lund-Andersen, "Vitreous fluorophotometry: Mathematical analysis of the efect of peripheral leakage on axial scans," *Invest. Ophthalmol. Vis. Sci.*, vol. 30, pp. 1522–1526, 1989.
[29] H. Lund-Andersen, B. Krogsaa, M. Cour, and J. Larsen, "Quantitative vitreous fluorometry applying a mathematical model of the eye," *Invest. Ophthalmol. Vis. Sci.*, vol. 26, pp. 689–710, 1985.
[30] M. Larsen, P. Dalgaard, and H. Lund-Andersen, "Differential spectrofluorometry in the human vitreous: Blood-retina barrier permeability to fluorescein and fluorescein glucuronide," *Graefe's Arch. Clin. Exp. Ophthalmol.*, vol. 229, pp. 350–357, 1990.
[31] B. Sander, M. Larsen, B. Moldow, and H. Lund-Andersen, "Diabetic macular edema: Passive and active transport of fluorescein through the blood-retina barrier," *Invest. Ophthalmol. Vis. Sci.*, vol. 42, pp. 433–438, 2001.
[32] D. J. Spalton, R. A. Hitchings, and P. A. Hunter, *Atlas d'ophthalmologie clinique*, Paris: MEDSI, 1986, pp. 13.1–13.8.
[33] Matlab, Natick, MA. Matlab. [Online]. Available: http://www.mathworks.com

Rui Bernardes was born on November 15, 1965, in Coimbra, Portugal. He received the electrical engineer degree (specialization in computers) from the Faculty of Sciences and Technology, University of Coimbra on September 1992. He received the M.Sc. degree in biomedical engineering from the Faculty of Medicine, University of Coimbra, specialization in biomedical instrumentation, July 2000.

He is Director of the Center of New Technologies for Medicine (CNTM) of the Association for Innovation and Biomedical Research on Light and Image (AIBILI) since October 1999. His main research area is medical image processing, with activities and contributions in the field since 1999.

Jorge Dias was born on March 7, 1960, in Coimbra, Portugal. He received the electrical engineer degree (specialization in computers) from the Faculty of Sciences and Technology, University of Coimbra on July 1984. He received the Ph.D. degree in electrical engineering from the University of Coimbra, specialization in control and instrumentation in November 1994.

His main research area is Computer Vision, with activities and contributions in the field since 1984. He has been exploring different topics on Computer Vision in projects financed by the Portuguese institution JNICT—Junta Nacional de Investigação Científica, FCT—Portuguese Foundation for Science and Technology, European Community and NATO—Science For Stability.

José Cunha-Vaz was born on November 5, 1938, in Coimbra, Portugal. He received the M.D. degree from the Faculty of Medicine, University of Coimbra in 1962. He received the Ph.D. degree from the University of London, London, U.K., in 1965. He received the Doctor, Medical Science degree from the University of Coimbra, Portugal, in 1967.

He is Professor and Chairman, Department of Ophthalmology, Coimbra University Hospital, Dean, Faculty of Medicine at the University of Coimbra, Portugal and President of the Board of Administration of the Association for Innovation and Biomedical Research on Light and Image (AIBILI).